POLITECNICO DI TORINO
Repository ISTITUZIONALE

Mitigation of Residual Stress and Distortion of AlSi10Mg Parts Produced by Laser Powder Bed Fusion through a Proper Selection of Support Geometry

(Article begins on next page)

07 August 2024

ORIGINAL RESEARCH ARTICLE

Mitigation of Residual Stress and Distortion of AlSi10Mg Parts Produced by Laser Powder Bed Fusion through a Proper Selection of Support Geometry

Gabriele Piscopo (iD)*, Eleonora Atzeni, and Alessandro Salmi*

Laser beam powder bed fusion (LB-PBF) is an edge additive manufacturing technology that allows complex near-net shape components to be produced. The freedom of design of the LB-PBF process makes it possible to produce optimized geometries, driving the application of this process in sectors in which high performance is fundamental such as aerospace and automotive. However, the building process inherently generates residual stresses in the part and the use of support structures become essential to anchor the part to the building platform and avoid problems in the downfacing surfaces that may warp or collapse during the production process. In this paper, different support densities obtained using different geometries of support structures are investigated to evaluate how they affect the residual stress distribution in the supported part. Two families of support structures were considered, linear-type and volumetric-type, including also a hybrid support structure that combined a massive volume topped by a linear support structure. Results highlighted that the combined choice of support density and geometry influences the magnitude and the distribution of sub-superficial residual stresses near the support-part interface and that appropriate design is essential to prevent excessive distortion or failure.

1. Introduction

The complexity and quality of products that can be manufactured with modern additive manufacturing (AM) systems make the AM process increasingly competitive. In particular, nowadays it is possible to produce, without the use of tools (Ref 1, 2), near-net-shape parts with complex features and advanced materials. These technological advancements have impressively increased the end-use application of AM products in sectors such as aerospace (Ref 3, 4), automotive (Ref 5, 6) and medical (Ref 7, 8). Among the various metal AM processes currently available, Laser Beam-Powder Bed Fusion (LB-PBF) process is the most used thanks to its potentialities and flexibility that allow parts to be produced sustainably and with enhanced properties (Ref 2, 9-11). Despite the huge

number of benefits, there are still some issues that have to be addressed to improve part quality and repeatability, mechanical properties, and residual stress state (Ref 12-14). As a matter of fact, it is well known that AM processes that use a laser as an energy source are characterized by high-temperature gradients (Ref 15-17) that cause high levels of residual stresses.

The production of the complex AM geometries requires the use of support structures (Ref 18, 19). Support structures allow to anchor the part to the building platform and reduce the distortion caused by thermal warping and phase transformation (Ref 20). However, supports are additional volumes that inevitably increase production time and cost, and have to be removed after building, thus constituting waste material. In this regard, designers privilege the minimal use of supports able to counteract residual stress release and consequent part deformation during the building process. As a matter of fact, the residual stresses generated in LB-PBF processes, if not taken in account in the process design, can even induce the formation of cracks and delamination between layers which, in most cases, cause the failure of the manufacturing process (Ref 21-23). Due to the relevance of the residual stress state of AM components, several studies were performed in order to understand and quantify the residual stress distribution in as-built samples. According to Withers and Bhadeshia (Ref 24), the origin of residual stress is related to phase transformation and to non-uniform plastic deformation. Withers and Bhadeshia (Ref 25) defined three different types of residual stress that act at different part scales, that are the macroscopic scale, the microscopic scale, and the atomic scale. Especially stresses acting on a macroscopic scale have been discussed and analyzed in the literature since they are responsible of distortion of the whole component and reduction of fatigue properties (Ref 26). Nowadays, it is commonly accepted that on the top

Gabriele Piscopo, Eleonora Atzeni, and **Alessandro Salmi**, Department of Management and Production Engineering, Politecnico di Torino, Corso Duca Degli Abruzzi, 24, 10129 Torino, Italy. Contact e-mail: gabriele.piscopo@polito.it.

and the bottom surfaces, a tensile residual stress is obtained; instead, the core is characterized by a compressive stress state (Ref 27). In addition, the stresses parallel to the scanning direction are almost twice with respect to those in the traverse direction (Ref 26).

The residual stresses developed in a part during building can be partially controlled through a proper selection of process parameters and an optimal design of the same part to achieves better heat transfer and distribution. For example, Yu et al. (Ref 28) showed that, in 7075 aluminum alloys, thermal residual stresses which led to solidification cracks were reduced by a proper selection of the process parameters and with the introduction of 1% w.t. Zr. However, it is not possible to eliminate residual stresses, and a further optimization should be carried out by a proper design of support structures. Salmi and Atzeni (Ref 29) analyzed the stress state in AlSi10Mg samples produced by the LB-PBF process at different process phases and also the effect of support structures. They observed that the mere presence of support structures between the building platform and the part increases the level of residual stresses, compared to those measured on samples that show geometric continuity to the substrate. Other studies analyzed the support structure strength for different support types. In fact, the strength of the support structure should be high enough to prevent part warping (Ref 30). Hussein et al. (Ref 31) performed one of the first experimental investigation to relate lattice support structures to part manufacturability, building time and material waste. In their investigation different lattice support structures, such as gyroid and Schwartz diamond structures, were analyzed by varying cell size and volume fraction. They showed that lattice support structures allow a significant material saving up to 92% with respect to solid supports, however they are often too fragile to be printed properly. Liu et al. (Ref 27) showed that the block support structure, typically used in the LB-PBF process, can be optimized in terms of geometrical parameters, and a decrease in the hatching distance and an increase in teeth size at the periphery of the component could prevent the part from warping. Xiaohui et al. (Ref 32) optimized the design of block support structures type to improve component stiffness. They showed that the density of the support structure and the contact area between the support tooth and the component greatly influence the stiffness of the overhang structure. Khobzi et al. (Ref 33) using a numerical simulation, showed that the contact area had a strong influence on the deformation of the component. On the other hand, they observed that the height of the teeth had no significant effect on the deformation. Subedi et al. (Ref 34) used the equivalent static load (ESL) to design and optimize tree-type support structures. They showed that by optimizing the support structure a better thermal transient was obtained and this could prevent job failure due to part warping. Mele et al. (Ref 35) correlated the overhang geometrical parameters with the support structures characteristics. In their work the effect of the density of linear support structures on sample warping was investigated. They showed that the design of the support structure should be carried out considering the thickness and the inclination of the overhang. Weber et al. (Ref 36) used Ansys to evaluate the effect of geometrical parameters of tree supports on the maximum displacement of a cantilever sample after cool-down. Results showed that the most important parameters were the trunk diameter and the distance between branches. Similarly, Weber et al. (Ref 37) evaluated the geometrical characteristics of tree supports and it emerged

that the support strength was mainly influenced by trunk and branch diameter and by the number of branches. Gülcan et al. (Ref 38) investigated the effect of support tooth characteristics, such as tooth height, top length, base length, and base interval on the dimensional accuracy, roughness, hardness and support volume. Results revealed that the tooth height was the most influencing parameter on support volume and dimensional accuracy. In particular, a lower support volume and a lower dimensional accuracy were obtained by increasing the tooth height.

From the analysis of the literature review, it emerges a great interest in support structure optimization to find a good balance between support volume and strength. The geometrical parameters of different types of support structures have been analyzed to understand how to prevent part distortion. However, residual stresses are influenced by the presence and type of support structures, and the analysis of this cause-effect relationship is the objective of this paper. In detail, in this work AlSi10Mg parallelepiped samples were produced with different density and geometry of support structures to evaluate their effect on the residual stresses developed near the support-part interface. The geometries of the support structures have been selected using the geometries typically available in commercial software libraries. This was done in order to adopt a practical approach that could be used by a user when preparing the job. Two families of support structures were evaluated, linear-type and volumetric-type, plus a hybrid support structure that combines linear supports and an underlying solid volume. After production, residual stresses were experimentally evaluated using the hole-drilling strain gauge method to relate the magnitude and the distribution of residual stresses to the density and geometry of the support structures.

2. Support Structure Types and Geometries

Considering the typical support features used in LB-PBF, seven different support structure geometries can be identified: block, contour, web, hybrid, tree, cone, and volume (Fig. 1).

Block supports have a grid structure, that is defined by the spacing (hatching) between two parallel lines, which can be changed between rows and columns independently. The contour supports consist of several walls that replicate the contour of the supported surface. The distance between two consecutive walls is defined by the offset parameter. Web supports are composed of a bundle of radial walls (ribs) and a certain number of circular walls. The length of the ribs is defined by the radius, the spacing between the circular walls is defined by the hatching distance. The hybrid support structure is composed of a solid base growing directly on the substrate and block supports that connect the solid base and the sample. Tree support structures are relatively new support structures developed to minimize the support density (Ref 39). They consist of a trunk and several branches, both defined by the minimum and the maximum diameter. The distribution of the tree structures is defined by the minimum and the maximum distances between connection points and by the minimum distance between rows. Cone supports consist of several vertical truncated cones geometrically defined by the radius at the interface with the part and by the radius at the platform. The spatial distribution of the cones is defined through the minimum and maximum distances between two adjacent cones, and the
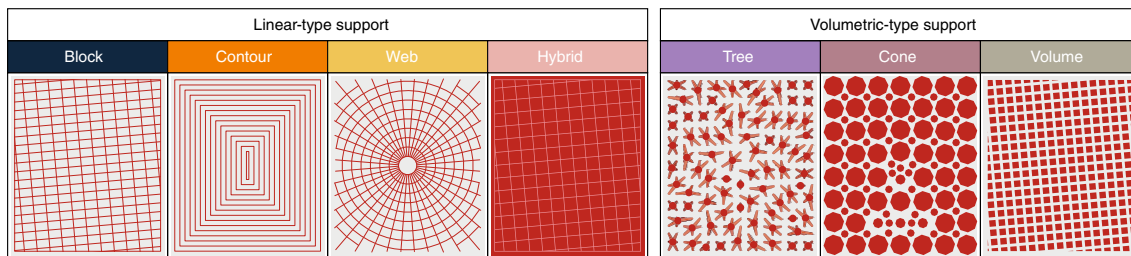
Fig. 1 Bottom view of the different support structure geometries

minimum distance between rows. Volume supports are basically composed of a matrix of rectangular struts that connects the sample to the substrate. The volume support is fragmented defining the dimension of the strut and the separation width between the struts.

Based on the geometry and the nature of the support structures, they can be classified into two families: linear-type support structures, namely block, contour, web and hybrid types, and volumetric-type support structures, namely tree, cone, and volume. It is worth noting that linear supports are preferable when the main objective is the reduction of material, cost and building time related to supports, and to facilitate the removal of the same support structures. However, contact with the supported surface of the part is limited to the teeth at the interface, resulting in less heat transfer and less resistance to detachment. Cone and volume supports are generally more robust and are preferred when greater heat dissipation or strength are required, but they typically involve a higher density of supports. Tree support structures are volumetric supports that have been developed to minimize support density. Hybrid supports limit the height of linear-type supports near the supported surface and provide a solid material (which could be also topology optimized for material saving) underneath to increase robustness while providing ease of removal. They thus represent a compromise between linear-type and volumetric-type support structures.

3. Materials and Method

In the following sections, the experimental procedure used to relate the residual stresses to the support density and geometry is described. The designed sample geometry and the geometrical parameters of support structures are specified. The method and the equipment used to produce the samples and to measure the residual stress distribution are then described.

3.1 Sample Geometry and Support Structures

The size of the sample was chosen to meet the minimum requirement of residual stress evaluation by the hole drilling method (Ref 40). Specifically, a $12 \times 14 \times 14$ mm3 parallelepiped sample was designed for the experimental campaign (Fig. 2a). A small section is realized, with the consideration that an effect visible on this scale will be certainly amplified on larger scales.

The seven geometries of support structures previously described were generated using Magics v26 software (Materialise, Leuven, Belgium), locating the sample at 5 mm above the substrate, and targeting the relative densities as 10% for tree

structures, 20% for linear-type structures (excluding hybrid type), 30% for hybrid structure, and 40% for the remaining volumetric-type support structures.

Table 1 summarizes the geometrical parameters of the support structures and their values and the corresponding relative densities. Considering linear-type supports, the connection teeth between the support structure and the part were kept at the default dimensions, so as not to introduce additional geometrical parameters.

3.2 Sample Production

A commercial AlSi10Mg (CL31 Al) alloy provided by Concept Laser was used to produce the supported parallelepiped samples. Two replicas of the samples, 7 samples each, were produced in a single job using a Mlab R Cusing system (GE Additive, Lichtenfels, Germany). This LB-PBF system was characterized by a 100-W fiber laser and a spot diameter in the focal plane of 100 μm. During the building process, a level of oxygen lower than 0.1% was guaranteed in the building chamber through a constant flow of Argon.

In order to achieve complete densification, the default process parameters recommended by the system manufacturer for the AlSi10Mg material were used for the production (Table 2). The alternating island exposure scanning strategy was characterized by an island size of 5 mm. The scanning vector was rotated by an angle of 90° between neighboring islands and, at each layer, a shifting of 1 mm of the islands in both the X and the Y directions was applied. Support structures were produced with the same process parameters used for the contour.

The first replica of samples was then removed from the building platform using wire-electrical discharge machining (W-EDM) in order to analyze the residual stress state in the as-built condition. The cut was located 1 mm from the platform, keeping the support connected to the part. The second replica of samples was subjected to a stress-relieving heat treatment at 310 °C for 1 hour and subsequently was removed from the building platform by the W-EDM process, for further residual stress analysis.

3.3 Residual Stress Measurement

For each sample of the two replicas, the residual stress distribution was measured on the lateral surface 5 mm above the bottom edge (Fig. 2b). The lateral surface was chosen since the higher residual stresses, which could lead to support failure, are generally observed at the periphery of overhang structures. The distance from the support where residual stresses were measured was selected to be as close as possible the support-part interface, while minimizing edge effects in the evaluation. The MTS3000 Restan system (SITN Technology s.r.l., Calen-
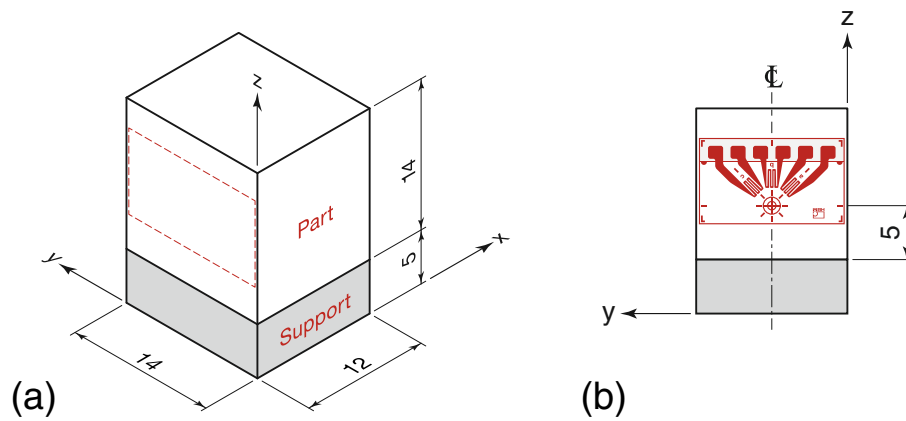
Fig. 2 Sample dimension and position of the strain gage rosette on the lateral surface

Table 1 Geometrical parameters and values of the support structures

Type	Geometry	ID	Parameters	Values	Density, %
Linear	Block	LB	Hatching	0.68 mm × 1 mm	22
	Contour	LC	Offset	0.4 mm	
	Web	LW	No. of ribs	20	
			Radius	2 mm	
			Hatching	0.73 mm	
	Hybrid (Block + Solid)	LH	Block hatching	1 mm × 1 mm	32
			Solid dimensions	12 mm × 14 mm × 1 mm	
Volumetric	Tree	VT	Top trunk diameter	0.4 mm	10
			Bottom trunk diameter	0.6 mm	
			Top branch diameter	0.2 mm	
			Bottom branch diameter	0.3 mm	
			No. of branches per track	6	
			Min connection point distance	0.3 mm	
			Min row distance	0.3 mm	
			Max distance	0.6 mm	
	Cone	VC	Contact part diameter	0.25 mm	43
			Contact platform diameter	0.5 mm	
			Min row distance	0.1 mm	
			Min cone distance	0.1 mm	
			Max distance	0.2 mm	
	Volume	VV	Fragmentation	0.5 mm × 0.5 mm	45
			Separation width	0.23 mm	

Table 2 Process parameters used for the production of the samples

	Parameter	Value
	Layer thickness, μm	15
	Beam diameter, μm	100
Core	Power, W	95
	Scanning speed, mm/s	650
	Hatching distance, mm	0.105
	Island size, mm	5
	Island shift, mm	1
Contour/support	Power, W	95
	Scanning speed, mm/s	1000
	Hatching distance, mm	0.105

zano, Italy) was used for residual stresses measurements. This system is based on the hole-drilling strain-gage method (HDM) which is recognized as one of the most efficient ones for evaluating residual stress distribution, in terms of cost, accuracy and versatility (Ref 40, 41). In HDM, a drilling cutter is used to produce a hole into the material to be tested. The hole is produced through a sequence of drilling steps. At each drilling step, a certain quantity of stressed material is removed, and this causes a localized deformation. This deformation is acquired at each drilling step by at least three elements of the rosette and the acquired deformations are used to back-calculate the residual stresses values according to the procedure detailed in the E837-20 ASTM Standard (Ref 40).

The surface of the specimen was manually prepared for the installation of the K-RY61-1.5/120R (HBM Italia s.r.l., Milano, Italy) Type B 3-element strain gauge rosette by removing the impurities (i.e., oxides) using silicon carbide paper. The surface

preparation was performed in two consecutive steps, using 200 grit silicon carbide paper and 400 grit silicon carbide paper in sequence to obtain a smooth surface (Ref 41). The surface was then cleaned from contaminants and dust using RMS1-SPRAY (HBM Italia s.r.l., Milano, Italy). The BCY01 (HBM Italia s.r.l., Milano, Italy) accelerator was applied on the tested surface in order to optimize the gluing operations that were performed using Z70 (HBM Italia s.r.l., Milano, Italy) cold curing superglue. The rosettes were then tested in order to verify the connection. A 1.8-mm-diameter coated carbide end mill with an inverted cone shape driven by a high-speed air turbine system was used to generate a 1.2 mm depth flat-bottom hole. The drilling operation was carried out with 4 drilling steps at a depth step of 25 μm, for more accurate measurement beneath the surface, followed by 20 drilling steps at a depth step of 50 μm, according to the ASTM Standard (Ref 40). The strain distribution was introduced in the EVAL software that allows calculating the residual stress according to ASTM E837-20 (Ref 40).

4. Results and Discussion

In the following sections, the results obtained from the residual stress measurements are described. The residual stresses of each sample are presented in terms of the maximum principal stress (σ_{max}), the minimum principal stress (σ_{min}) and the direction of principal stress (β). The combination of these three parameters allows to univocally define the tensional state of the sample. In addition, the software used for residual stress evaluation considers all the most important sources of uncertainties such as material density measurement, strain gage error, and hole eccentricity, thus providing the tolerance bounds for the residual stress curves. Then, a comparative analysis was performed to distinguish similarities and differences on residual stress behaviors.

4.1 Residual Stress Distribution on as-Built Samples

The production of all the samples was completed, however some warping was observed at the bottom of the LC and LW Samples produced with the contour and web linear type supports, with corners detached from the support structures (Fig. 3). Especially the web support structure was not adequate to anchor the part and the deformation was very pronounced, so the LW Sample was excluded from the residual stresses evaluation phase. In samples with volumetric supports, minor distortion was observed only at the corners of VT Sample. Residual stress distributions are described in the following sections by distinguishing the two support structure families,

that are the linear-type and the volumetric-type support structures. Then, the residual stresses measured on heat-treated samples are presented.

4.1.1 Effect of Linear-type Support Structures on Residual Stress Distribution. The residual stress distributions of linear-type support structures are depicted in Fig. 4(a). It is possible to observe that all samples were characterized by a tensile residual stress. The maximum principal stress σ_{max} ranged from 155 to 255 MPa, excluding the LH sample, produced with the hybrid support structure, that showed a value of about 100 MPa at the surface. The minimum principal stress σ_{min} ranged from 50 to 95 MPa. The highest residual stress values were observed in the LC Sample produced with the contour support structure. As a matter of fact, this sample showed local detachment from supports at the corners (which are the most stressed areas of the part), with visible warping. It is worth noting that part deformation, allowed by the failure of supports, locally relieved residual stresses and affected the value measured at the surface. In the LC Sample, the peak stress (255 MPa) was measured at a depth of 0.125 mm from the surface, the surface σ_{max} value being about 200 MPa, and the σ_{max} stress value after the peak gradually reached a plateau of 155 MPa from a depth of 0.4 mm. The same plateau was observed in the other samples starting from (0.4-0.5) mm below the surface, with visible differences in stress state only at a depth near the surface. For this reason, the scale in Fig. 4 is limited to 0.5 mm depth. The block support structure generated in the LB sample a similar residual stress behavior, but with slightly lower σ_{max} values and slightly greater σ_{min} values in the near-subsurface. No warping was observed in this sample. For the same support density, the topology of the support structure has thus influenced the residual stress state. This difference could be related to the fact that support lines are connected to each other in the block support, but not in the contour type, leading to better temperature distribution and lower gradients at the contour of the sections during building. This observation also suggests that block support structures should be preferred to contour ones for the considered overhang area to improve the residual stress behavior, since they lead to a more homogeneous temperature distribution in the layers.

In the LH sample built with the hybrid support, the residual stress values are further reduced, with a significant decrease in the maximum principal stress σ_{max} at the surface. This support solution appears viable to avoid undesired support detachments on larger scanned areas, as heat transfer and temperature homogenization are improved, but at cost of larger support volumes, which imply higher costs and building time.

Finally, it could be observed that the support structure geometry did not significantly influence the direction of the maximum principal stress. For all support structures, the direction ranged between 40 and 50° with respect to *a*-gauge,
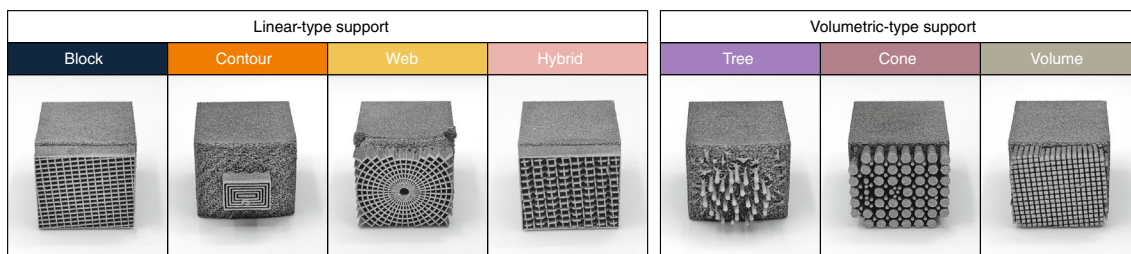
Linear-type support				Volumetric-type support		
Block	Contour	Web	Hybrid	Tree	Cone	Volume

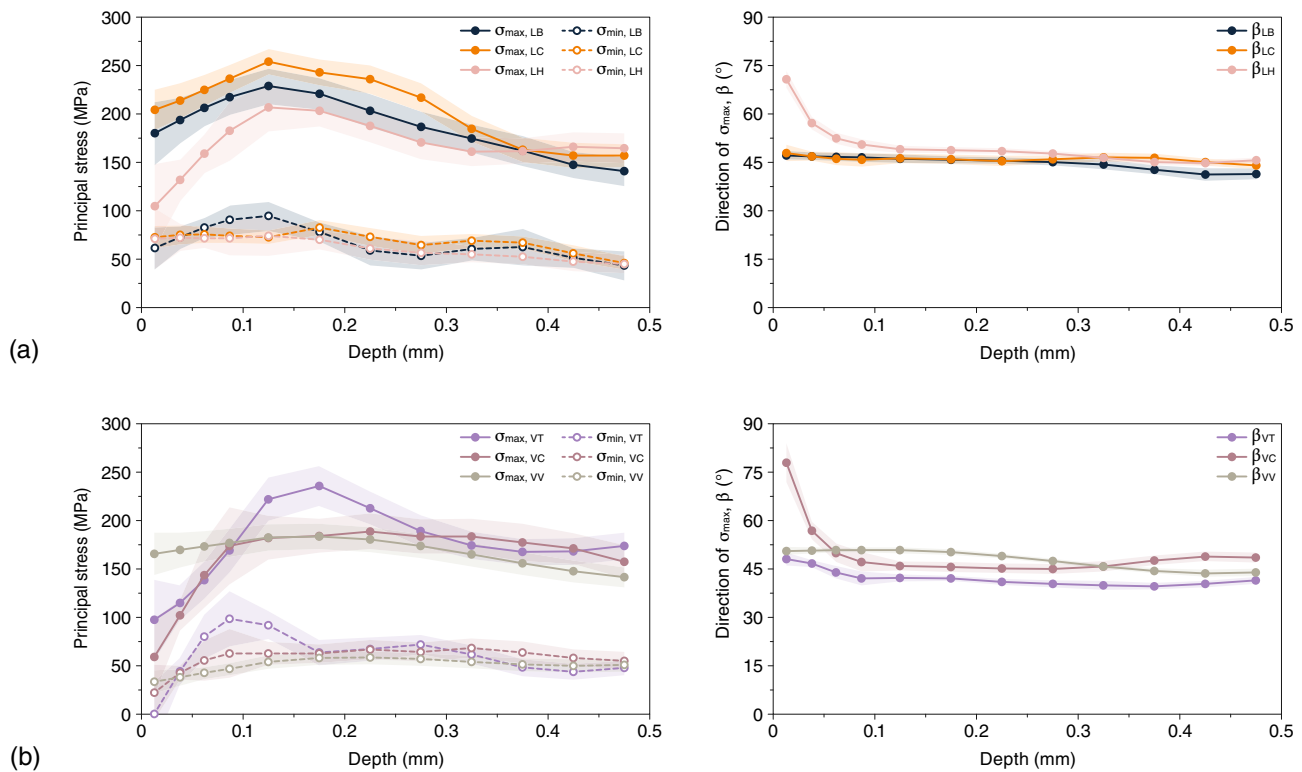**Fig. 3** Pictures of the samples after W-EDM cut at 1 mm from the substrate

Fig. 4 Residual stress distribution and maximum principal stress direction on as-built samples produced with (a) linear-type support structures and (b) volumetric-type support structures

which was oriented at 45° to the building direction. In other words, it is possible to state that the maximum principal stress was almost aligned with the building direction in all the samples analyzed.

4.1.2 Effect of Volumetric-type Support Structures on Residual Stress Distribution. The residual stress distributions of samples produced with different volumetric support structures are illustrated in Fig. 4(b). As expected considering this family of support structures, the highest residual stresses were measured in the VT Sample produced with the lowest support density and tree support structures. Some of the tree supports at the periphery detached from the part, and minor warping was observed at corners. Again, this affected the residual stress state, and the maximum principal stress σ_{max} measured at the surface was about 100 MPa. The stress σ_{max} rapidly increased near below the surface up to 236 MPa, measured at a depth of 0.175 mm. The absence of interconnections between trees combined with the small support volume had an adverse effect on temperature distribution and residual stresses.

The VC sample and the VV sample, built with cone and volume supports, respectively, were characterized by a similar residual stress distribution, which appears more homogeneous in the case of volume supports. This is desirable in the building process, as non-uniform stress distribution is closely related to non-homogeneous deformations on the produced part. Comparing these two support solutions, the lower value of σ_{max} observed at the surface in the VC sample is a consequence of the larger distance of the edges from the supports, the cone support structures being tapered upward, resulting in less constraint. The smaller contact area of the support with the part,

and the larger distance between connection points could explain the slightly higher stresses more in depth.

As observed in the samples with line support structure, also in this case the direction of the maximum principal stress was almost aligned with the building direction, with no significant influence of the support structure geometry.

4.1.3 Residual Stress Distribution on Heat Treated Samples. Figure 5 shows the stress distribution on samples after heat treatment for stress relieving. As expected, the heat treatment caused an overall reduction of stresses and all samples reached analogous stress state, independently from the geometry or density of support structures. The measured principal stresses ranged between 0 and 75 MPa. The effects of support structures and densities were thus lost after stress relieving; however, they influenced the building process, leading in some cases to building failure due to excessive part distortion.

5. Conclusion

In this work, the effect of different densities and geometries of support structures on the residual stress state of AlSi10Mg samples was investigated. The results showed that the stress distribution is influenced by density and the geometry of the support structures used during the building process. In detail, the main results obtained in this work can be summarized as follows:

- The block support geometry exhibited the best behavior among the linear-type supports. The web geometry of sup-
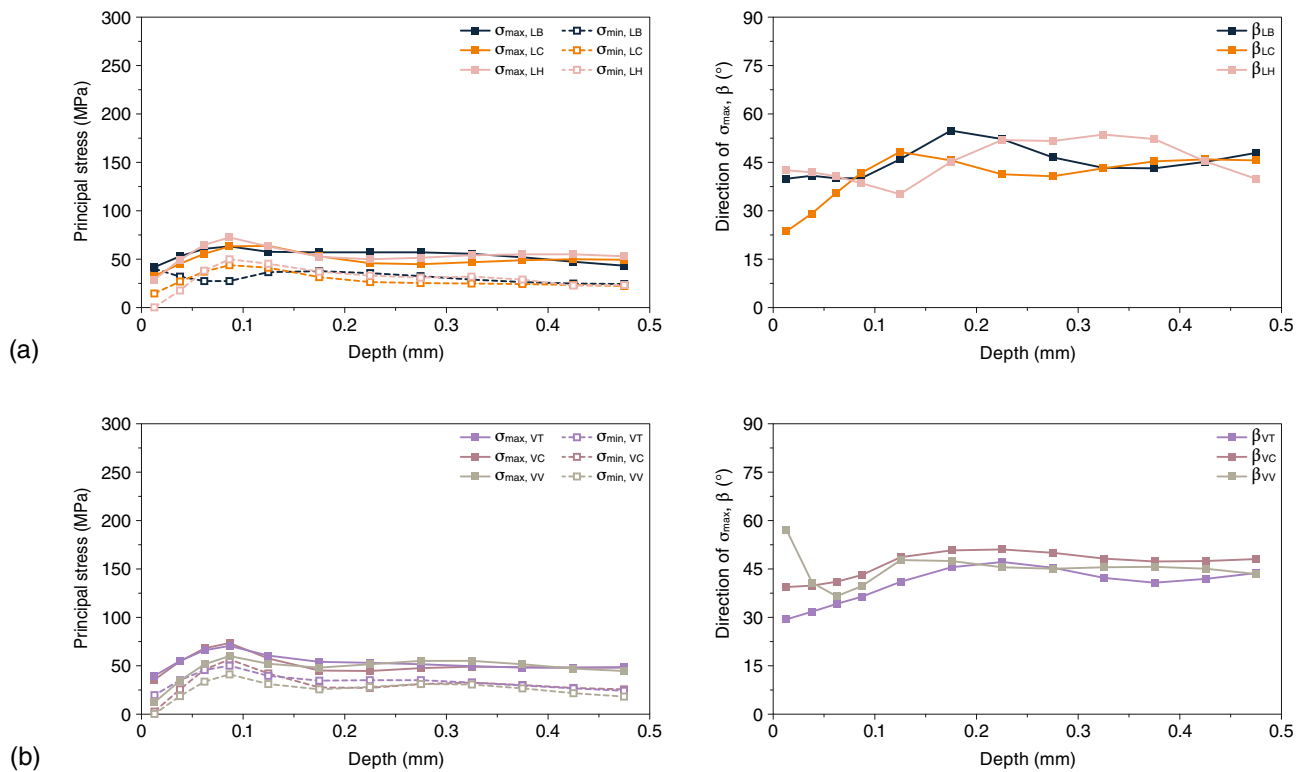
Fig. 5 Residual stress distribution and maximum principal stress direction on heat treated samples produced with (a) linear-type support structures and (b) volumetric-type support structures

port structure was not suitable for the production of the parallelepiped samples, and a significant warping was visible. The contour geometry of supports led to the higher stresses in the part, probably negatively affected by the lack of interconnection between the support walls.

- An interesting alternative to block supports alone is the combination of block supports with a solid substrate, which allows for improved heat transfer and temperature distribution thus reducing residual stresses in the part. However, the support density is higher and in this case the use of topology optimization techniques for substrate design should be considered.
- In samples supported by volumetric structures, stresses are influenced by the shape of the support elements, which in turn define the connection area at the support/part interface. Volume supports provided the most uniform stress distribution, at the cost of less easy removal. In general, the volumetric support structure performs better than the linear-type, but with obvious repercussions on post-processing phases and costs due to their higher density.
- Tree support structures allowed the support density to be drastically reduced, but negatively affected stress distribution, limiting the contact area and the support strength.

The heat treatment relieved residual stresses in all samples, regardless of the type of support used. Indeed, the effect of the support structure geometry is much more significant during the building phase, where higher values of stresses combined with lower support strength can lead to warping or delamination.

References

1. F. Calignano, D. Manfredi, E.P. Ambrosio, S. Biamino, M. Lombardi, E. Atzeni, A. Salmi, P. Minetola, L. Iuliano, and P. Fino, Overview on Additive Manufacturing Technologies, *Proc. IEEE*, 2017, **105**(4), p 593–612

2. T. Wohlers and R.I. Campbell, *Wohlers report 2017: 3D printing and additive manufacturing state of the industry: annual worldwide progress report*, Wohlers Associates, Incorporated, 2017

3. J.C. Najmon, S. Raeisi, and A. Tovar, Review of Additive Manufacturing Technologies and Applications in the Aerospace Industry, *Additive manufacturing for the aerospace industry*. Elsevier, Amsterdam, 2019, p 7–31

4. R. Liu, Z. Wang, T. Sparks, F. Liou, and J. Newkirk, 13 - Aerospace applications of laser additive manufacturing, *laser additive manufacturing*. M. Brandt Ed., Woodhead Publishing, Swaston, 2017, p 351–371

5. N. Guo and M.C. Leu, Additive Manufacturing: Technology, Applications and Research Needs, *Front. Mech. Eng.*, 2013, **8**(3), p 215–243

6. I. Gibson, The Changing Face of Additive Manufacturing, *J. Manuf. Technol. Manag.*, 2017, **28**(1), p 10–17

7. C.L. Ventola, Medical Applications for 3D Printing: Current and Projected Uses, *Pharm. Ther.*, 2014, **39**(10), p 704

8. M. Javaid and A. Haleem, Additive Manufacturing Applications in Medical Cases: A Literature based Review, *Alex. J. Med.*, 2018, **54**(4), p 411–422

9. G. Piscopo and L. Iuliano, Current research and Industrial Application of Laser Powder Directed Energy Deposition, *Int. J. Adv. Manuf. Technol.*, 2022, **119**(11–12), p 6893–6917

10. C.N. Kuo, C.K. Chua, P.C. Peng, Y.W. Chen, S.L. Sing, S. Huang, and Y.L. Su, Microstructure Evolution and Mechanical Property Response via 3D Printing Parameter Development of Al–Sc Alloy, *Virtual Phys. Prototyp.*, 2019, **15**(1), p 120–129

11. W. Yu, S.L. Sing, C.K. Chua, and X. Tian, Influence of Re-melting on Surface Roughness and Porosity of AlSi10Mg Parts Fabricated by Selective Laser Melting, *J. Alloy. Compd.*, 2019, **792**, p 574–581

12. A. Mussatto, R. Groarke, R.K. Vijayaraghavan, C. Hughes, M.A. Obeidi, M.N. Doğu, M.A. Yalçin, P.J. McNally, Y. Delaure, and D. Brabazon, Assessing Dependency of Part Properties on the Printing Location in Laser-powder Bed Fusion Metal Additive Manufacturing, *Mater. Today Commun.*, 2022, **30**, p 103209

13. D. Wang, L. Liu, G. Deng, C. Deng, Y. Bai, Y. Yang, W. Wu, J. Chen, Y. Liu, Y. Wang, X. Lin, and C. Han, Recent Progress on Additive Manufacturing of Multi-material Structures with Laser Powder Bed Fusion, *Virtual Phys. Prototyp.*, 2022, **17**(2), p 329–365

14. L. Dowling, J. Kennedy, S. O'Shaughnessy, and D. Trimble, A Review of Critical Repeatability and Reproducibility Issues in Powder Bed Fusion, *Mater. Design*, 2020, **186**, p 108346

15. Y. Chen and I.C. Sheng, Residual Stress in Weldment, *J. Therm. Stresses*, 1992, **15**(1), p 53–69

16. B. Yilbas and S. Akhtar, Laser Bending of Metal Sheet and Thermal Stress Analysis, *Opt. Laser Technol.*, 2014, **61**, p 34–44

17. Y.-S. Yang and S.-J. Na, A Study on Residual Stresses in Laser Surface Hardening of a Medium Carbon Steel, *Surf. Coat. Technol.*, 1989, **38**(3), p 311–324

18. D. Brackett, I. Ashcroft, and R. Hague, Topology optimization for additive manufacturing, Proceedings of the solid freeform fabrication symposium, 2011 (Austin), pp 348–362

19. G. Piscopo, A. Salmi, and E. Atzeni, On the Quality of Unsupported Overhangs Produced by Laser Powder Bed Fusion, *Int. J. Manuf. Res.*, 2019, **14**(2), p 198–216

20. M.X. Gan and C.H. Wong, Practical Support Structures for Selective Laser Melting, *J. Mater. Process. Tech.*, 2016, **238**, p 474–484

21. A. Salmi, G. Piscopo, E. Atzeni, P. Minetola, and L. Iuliano, On the Effect of Part Orientation on Stress Distribution in AlSi10Mg Specimens Fabricated by Laser Powder Bed Fusion (L-PBF), *Procedia CIRP*, 2018, **67**(1), p 191–196

22. E.O. Olakanmi, R.F. Cochrane, and K.W. Dalgarno, A Review on Selective Laser Sintering/Melting (SLS/SLM) of Aluminium Alloy Powders: Processing, Microstructure, and Properties, *Prog. Mater. Sci.. Mater Sci.*, 2015, **74**, p 401–477

23. K. Kempen, L. Thijs, B. Vrancken, S. Buls, J. Van Humbeeck, and J. Kruth, Producing crack-free, high density M2 HSS parts by selective laser melting: pre-heating the baseplate, Proc. 24th Int. Solid Free. Fabr. Symp, 2013 (Austin), pp. 131-139

24. P.J. Withers and H. Bhadeshia, Residual Stress. Part 2–Nature and Origins, *Mater. Sci. Technol.*, 2001, **17**(4), p 366–375

25. P.J. Withers and H. Bhadeshia, Residual Stress. Part 1–Measurement Techniques, *Mater. Sci. Technol.*, 2001, **17**(4), p 355–365

26. J.L. Bartlett and X. Li, An Overview of Residual Stresses in Metal Powder Bed Fusion, *Addit. Manuf.. Manuf.*, 2019, **27**, p 131–149

27. Y. Liu, Y. Yang, and D. Wang, A Study on the Residual Stress during Selective Laser Melting (SLM) of Metallic Powder, *Int. J. Adv. Manuf. Technol.*, 2016, **87**(1–4), p 647–656

28. W. Yu, Z. Xiao, X. Zhang, Y. Sun, P. Xue, S. Tan, Y. Wu, and H. Zheng, Processing and Characterization of Crack-free 7075 Aluminum Alloys with Elemental Zr Modification by Laser Powder Bed Fusion, *Mater. Sci. Addit. Manuf.*, 2022, **1**(1), p 4

29. A. Salmi and E. Atzeni, History of Residual Stresses during the Production Phases of AlSi10Mg Parts Processed by Powder Bed Additive Manufacturing Technology, *Virtual Phys. Prototyp.*, 2017, **12**(2), p 153–160

30. J. Zhang, Q. Cao, and W.F. Lu, A Review on Design and Removal of Support Structures in Metal Additive Manufacturing, *Mater. Today Proc.*, 2022, **70**, p 407–411

31. A. Hussein, L. Hao, C. Yan, R. Everson, and P. Young, Advanced Lattice Support Structures for Metal Additive Manufacturing, *J. Mater. Process. Technol.*, 2013, **213**(7), p 1019–1026

32. J. Xiaohui, Y. Chunbo, G. Honglan, G. Shan, and Z. Yong, Effect of Supporting Structure Design on Residual Stresses in Selective Laser Melting of AlSi10Mg, *Int. J. Adv. Manuf. Technol.*, 2021, **118**(5–6), p 1597–1608

33. A. Khobzi, F. FarhangMehr, S. Cockcroft, D. Maijer, S.L. Sing, and W.Y. Yeong, The Role of Block-type Support Structure Design on the Thermal Field and Deformation in Components Fabricated by Laser Powder Bed Fusion, *Addit. Manuf.. Manuf.*, 2022, **51**, p 102644

34. S.C. Subedi, A. Shahba, M. Thevamaran, D.J. Thoma, and K. Suresh, Towards the Optimal Design of Support Structures for Laser Powder Bed Fusion-Based Metal Additive Manufacturing via Thermal Equivalent Static Loads, *Addit. Manuf.. Manuf.*, 2022, **57**, p 102956

35. M. Mele, A. Bergmann, G. Campana, and T. Pilz, Experimental Investigation into the Effect of Supports and Overhangs on Accuracy and Roughness in Laser Powder Bed Fusion, *Optics Laser Technol.*, 2021, **140**, p 107024

36. S. Weber, J. Montero, M. Bleckmann, and K. Paetzold, Parametric Design Optimisation of Tree-like Support Structure for the Laser-based Powder Bed Fusion of Metals, *J. Manuf. Process.*, 2022, **84**, p 660–668

37. S. Weber, J. Montero, M. Bleckmann, and K. Paetzold, Parameters on Support Structure Design for Metal Additive Manufacturing, *Proc. Design Soc. Design Conf.*, 2020, **1**, p 1145–1154

38. O. Gülcan, K. Günaydın, A. Çelik, and E. Yasa, Optimization of Tooth Support Geometrical Parameters for Laser Powder Bed Fusion Produced Overhang Parts, *J. Test. Eval.Eval.*, 2023, **51**(2), p 961–978

39. Support generation, https://www.materialise.com/en/industrial/software/support-generation, Accessed 27 March 2023

40. "Standard Test Method for Determining Residual Stresses by the Hole-Drilling Strain-Gage Method," ASTM E837-20, ASTM International, 2020

41. G.S. Schajer, *Practical Residual Stress Measurement Methods*, Wiley, London, 2013